Journal of the European Ceramic Society **13** (1994) 453–460

Stresses Near the Free Edge of the Interface in Ceramic-to-Metal Joints

D. Munz & Y. Y. Yang

University of Karlsruhe, Institute for Reliability and Failure Analysis, Postfach 3640, D-76021 Karlsruhe, Germany

(Received 23 August 1993; revised version received 25 November 1993; accepted 14 December 1993)

Abstract

In ceramic to metal joints high stresses develop at the free edge of the interface under mechanical loading or after a change in temperature. These stresses can be described analytically by a singular stress term and a term which is independent of the distance from the free edge of a rectangular joint. All parameters in the stress expression can be calculated analytically. General rules on the effect of the material properties (elastic constants, thermal expansion coefficients) on the stresses can be deduced.

An Metall–Keramik-Verbindungen können an der freiliegenden Kante infolge mechanischer Belastung oder aufgrund eines Temperaturwechsels hohe Spannungen auftreten. Diese Spannungen lassen sich für einen Verbund mit rechteckigem Querschnitt analytisch durch einen singulären Term und einen Term, der vom Kantenabstand abhängt, beschreiben. Im Ausdruck für die Spannung können alle Parameter analytisch berechnet werden. Es lassen sich allgemeine Regeln für den Einfluß der Materialeigenschaften (elastische Konstanten, thermische Ausdehnungskoeffizienten) ableiten.

Dans certains joints céramique–métal, des contraintes élevées se développent au niveau du bord libre de l'interface, sous charge, ou après un changement de température. On peut décrire analytiquement ces contraintes par un terme singulier et un terme indépendant de la distance au bord, ceci pour un joint rectangulaire. Tous les paramètres de l'expression donnant la contrainte peuvent être calculés analytiquement. On peut en déduire des règles générales sur l'effet des propriétés du matériau (constantes élastiques, coefficients d'expansion thermique) sur les contraintes.

1 Introduction

If ceramics are bonded to metals high stresses occur at the free edge of the interface under mechanical loading or after a change in temperature. The thermal stresses are caused by the different thermal expansions of the two materials and they are of importance, above all if bonding takes place at high temperatures. The stresses for a given geometry are dependent on the properties of the two bonded materials. For proper material selection the effect of these properties on the stress distribution near the free edge of the interface must be known. The stresses near the free edge of the interface have been calculated in several investigations. The first extensive treatment of the stress singularity was performed by Bogy;[1] it was based on an earlier publication by Williams.[2]

2 General relation

A plane problem is considered with the geometric parameters shown in Fig. 1. The joint has contact angles of 90°, a length of $2L$ and heights H_1 and H_2 of the ceramic (material 1) and the metal (material 2). A Cartesian x–y- or a polar r–θ-coordinate system is used. The following assumptions are made:

—Perfect bonding between metal and ceramic;
—isotropic, linear-elastic behaviour;
—temperature-independent material properties.

The assumption of elastic behaviour is not fulfilled very close to the free edge where very high stresses occur. Nevertheless, elastic calculations can show the general effect of the material properties, and very often the plastic zone may be only small. The stresses near the free edge can be

Journal of the European Ceramic Society 0955-2219/94/$7.00

described by[3,4]

$$\sigma_{ij}(r, \theta) = \frac{K_L}{(r/L)^{\omega}} f_{ij}(\theta) + \sigma_0 f_{ij0}(\theta) \qquad (1)$$

The distance r is related to the length parameter L (see Fig. 1). ω is the stress exponent, which is positive for most material combinations. This means that a stress singularity exists. ω depends on the elastic constants of the two materials (Young's moduli E_1 and E_2 and Poisson's ratios υ_1 and υ_2) and can be obtained from the relation given in the Appendix. The dependency on the four elastic constants can be reduced to the two Dundurs parameters, also given in the Appendix. For $\upsilon_1 \neq \upsilon_2$ a range of ratios exists of the Young's moduli for which ω is negative. The stress then is not singular; however, eqn (1) is still valid. This is shown in Fig. 2, where ω is plotted versus the relative difference of the effective Young's moduli E_i^* with

$$E_i^* = \begin{cases} \dfrac{E_i}{\upsilon_i} & \text{for plane stress} \\ \dfrac{E_i}{\upsilon_i(1+\upsilon_i)} & \text{for plane strain} \end{cases} \qquad (2)$$

f_{ij} are functions of θ and of the Dundurs parameters, which are given in the appendix. These relations were obtained from the general treatment of the problem as it was formulated by Williams.[2] For details see Yang.[5] K_L is the stress intensity factor, which is dependent on elastic properties and on the external loading. The definition of K_L differs from that in fracture mechanics. The advantage of the definition in eqn (1) is that the dimension of K_L is expressed as a stress. In connection with K_L the angular functions are defined such that $f_\theta = 1$ for $\theta = 0$. The second term in eqn (1) is zero for mechanical loading (the only exceptions are cracks), but it is very important for thermal loading. In Cartesian coordinates $f_{x0} = f_{xy0} = 0$ and $f_{y0} = 1$. The stress intensity factor K_L and the quantity σ_0 are proportional to change in temperature and proportional to $\Delta\alpha$, with

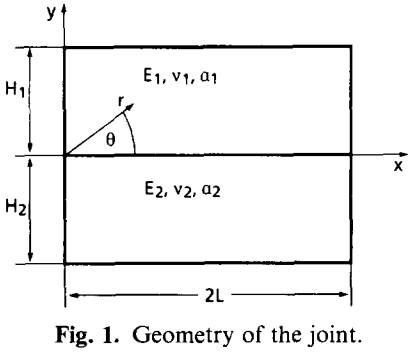

Fig. 1. Geometry of the joint.

$$\Delta\alpha = \begin{cases} \alpha_1 - \alpha_2 & \text{for plane stress} \\ \alpha_1(1+\upsilon_1) - \alpha_2(1+\upsilon_2) & \text{for plane strain} \end{cases} \qquad (3)$$

The constant stress term σ_0 is given by[3]

$$\sigma_0 = \Delta T \,.\, \Delta\alpha \,.\, \left[\frac{1}{E_1^*} - \frac{1}{E_2^*}\right]^{-1} \qquad (4)$$

The stress intensity factor has to be determined from numerical stress analysis. It could be shown[4] that for all possible material combinations a relation between the ratio K_L/σ_0 and the stress exponent ω exists if $H_1/L \geq 2$ and $H_2/L \geq 2$, which can be expressed as

$$-\frac{K_L}{\sigma_0} = 1 - 2{\cdot}89\omega + 11{\cdot}4\omega^2 - 51{\cdot}9\omega^3 + 135{\cdot}7\omega^4 - 135{\cdot}8\omega^5 \qquad (5)$$

From eqn (4) it can be seen that σ_0 approaches infinity if $E_1^* - E_2^*$ approaches zero. For this specific material combination the stress exponent ω is zero. The stress intensity factor K_L also approaches infinity with a sign different from that of σ_0. The ratio K_L/σ_0 is -1 for $\omega = 0$; thus, the stresses remain finite. For mechanical loading with a stress σ_∞ perpendicular to the interface, the effect of the material properties on K_L can be expressed by the same relation as for thermal loading, replacing $-K_L/\sigma_0$ in eqn (5) by K_L/σ_∞.

With eqns (1)–(5) the complete stress field near the free edge of the interface can be calculated for a change in temperature or for a mechanical load perpendicular to the interface without performing any further finite element calculation.

It should be mentioned that in eqn (1) r could also be related to another size parameter, for instance H_1. Then the stress intensity factor K_{H_1} would differ from K_L. Between K_L and K_{H_1} the relation exists:

$$K_{H_1} H_1^{\omega} = K_L L^{\omega} \qquad (6)$$

It is, however, useful to use K_L, because K_L is size

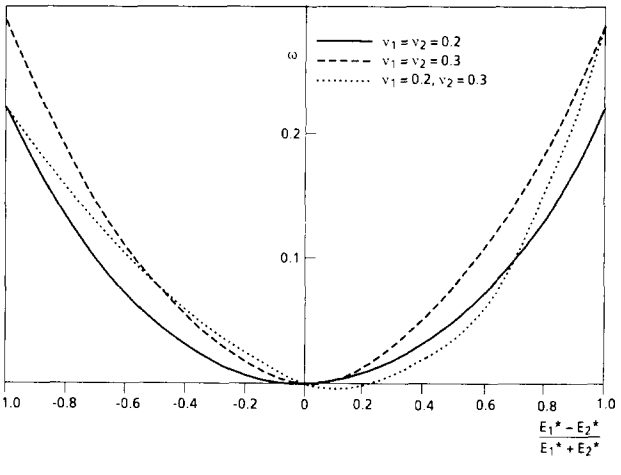

Fig. 2. Stress exponent versus relative difference of the effective Young's moduli.

Table 1. Properties of various materials

	E (GPa)	ν	$\frac{E}{\nu(1+\nu)}$ (GPa)	α ($\times 10^{-6}$/K)	$\alpha(1+\nu)$ ($\times 10^{-6}$/K)
Al_2O_3	375	0·27	1094	8·2	10·4
Al_2TiO_5	30	0·24	101	3·5	4·3
B_4C	390	0·15	2261	4·5	5·2
BeO	360	0·25	1152	8·7	10·9
MgO	295	0·36	603	13·6	18·5
$MoSi_2$	380	0·17	1910	8·5	9·9
SiC	410	0·24	1378	5·0	6·2
Si_3N_4-HP	314	0·28	876	2·7	3·5
TiC	318	0·19	1406	7·7	9·1
ZrO_2	240	0·30	615	11·0	14·3
Al	71	0·35	150	23·5	31·7
Al alloy	71	0·33	162	22·5	29·9
Cu	130	0·34	285	17·0	22·8
Ni	210	0·31	517	13·3	17·4
Nb	105	0·40	188	7·2	10·1
Mo	325	0·29	869	5·1	6·6
W	411	0·28	1147	4·5	5·8
Carbon steel	215	0·28	592	11·5	14·8
SS steel	200	0·30	513	16·0	20·8
Ti–6Al–4V	110	0·31	271	5·8	7·6
Ag–Ti braze	72	0·30	185	18·95	24·6

independent for $H_1/L \geq 2$ and $H_2/L \geq 2$, whereas K_{H_1} depends on H_1.

3 Results

In Table 1 the Young's moduli E, the Poisson's ratios ν and the thermal expansion coefficients α are listed for several ceramic and metal materials. Especially for the ceramics these properties depend strongly on the fabrication process and especially on the density of the material. The data in Table 1 are therefore representative values. In Fig. 3 the effective modulus E^* is plotted versus the effective thermal expansion coefficient for plane strain $\alpha^* = \alpha\ (1 + \nu)$. It can be seen that the ceramics have generally higher effective moduli and lower thermal expansion coefficients than the metals. There are, however, exceptions, e.g. molybdenum and tungsten, having a high modulus and a low thermal expansion, or the titanium alloy, whose thermal expansion and modulus are low.

As an example of the complete stress state in a joint finite element, results for the combination of alumina with the Ti–6Al–4V titanium alloy are shown in Fig. 4 for mechanical loading and in Fig. 5 for thermal loading. The stresses are plotted as a function of the distance from the free edge along the interface and along the free edge of the joint. For both loadings all stress components increase rapidly as the free edge of the interface is

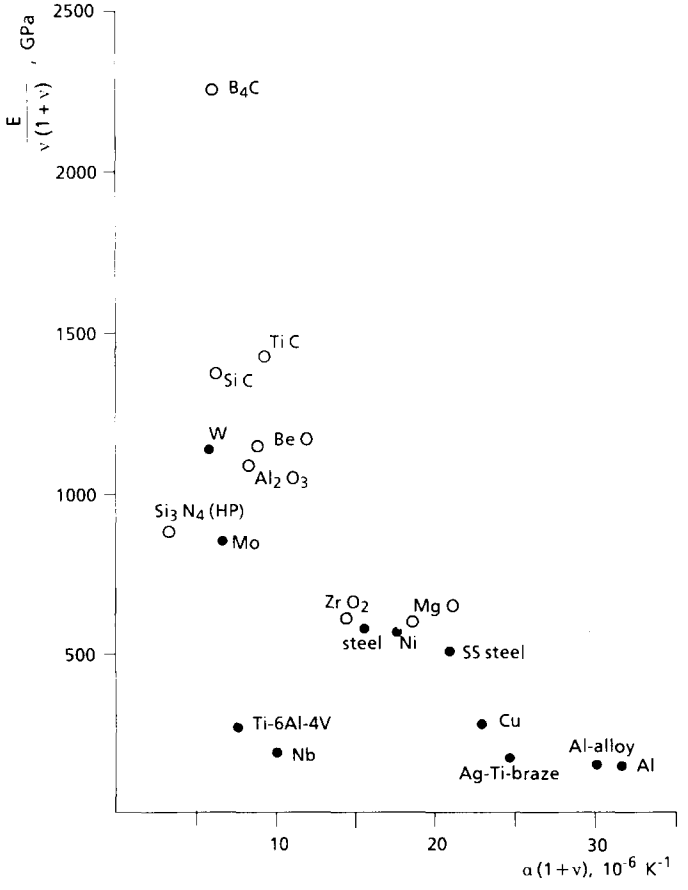

Fig. 3. Effective Young's modulus versus effective thermal expansion for some ceramics and metals.

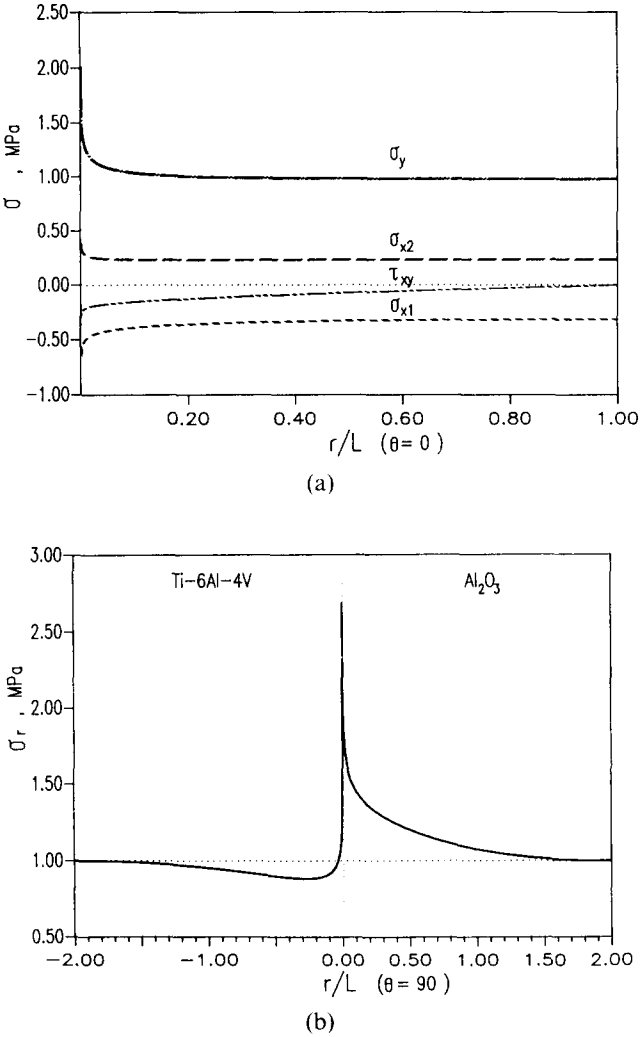

Fig. 4. Stresses along (a) the interface and (b) the free edge under mechanical loading (Al_2O_3/Ti–6Al–4V) (σ_∞ = 1 MPa).

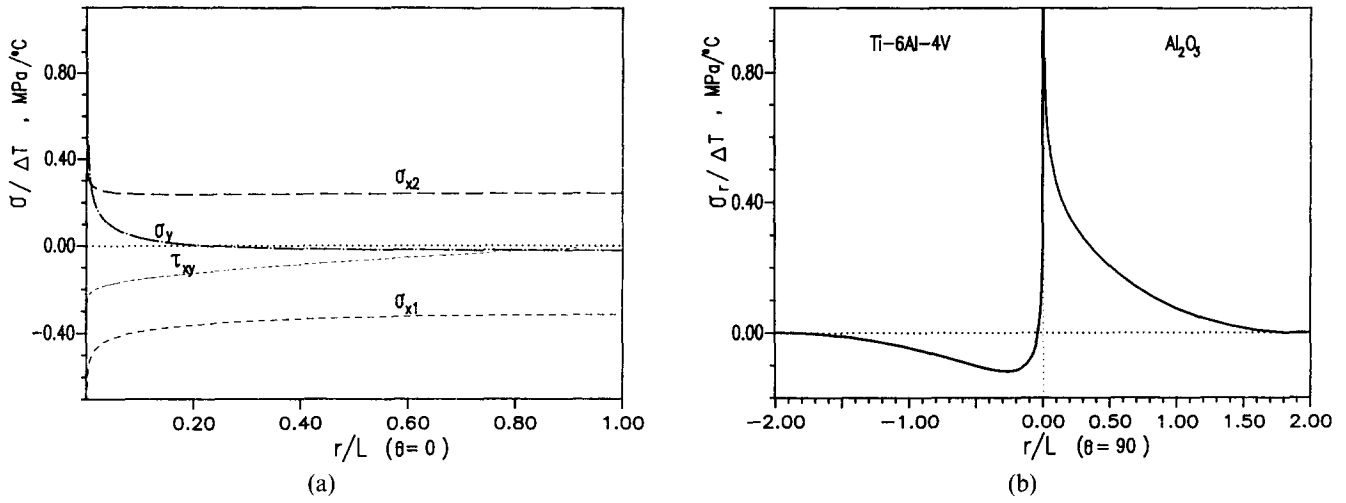

Fig. 5. Stresses along (a) the interface and (b) the free edge under thermal loading (Al_2O_3/Ti–6Al–4V).

approached. Under thermal loading the stress component σ_y along the interface changes its sign when approaching the free edge. Along the free edge the sign changes in the titanium alloy under thermal loading, but not in the alumina.

Equation (1) describes the stress distribution near the free edge of the interface. In Fig. 6 finite element results and the analytical results of eqn (1) are compared. It can be seen that along the free edge the results of eqn (1) have a deviation from the finite element results at about $r/L = 0{\cdot}1$. In Fig. 7 the results obtained under mechanical loading for different material combinations are shown. The stresses σ_y along the interface increase with increasing stress exponent ω. This follows from eqns (1) and (5). The constant stress term is

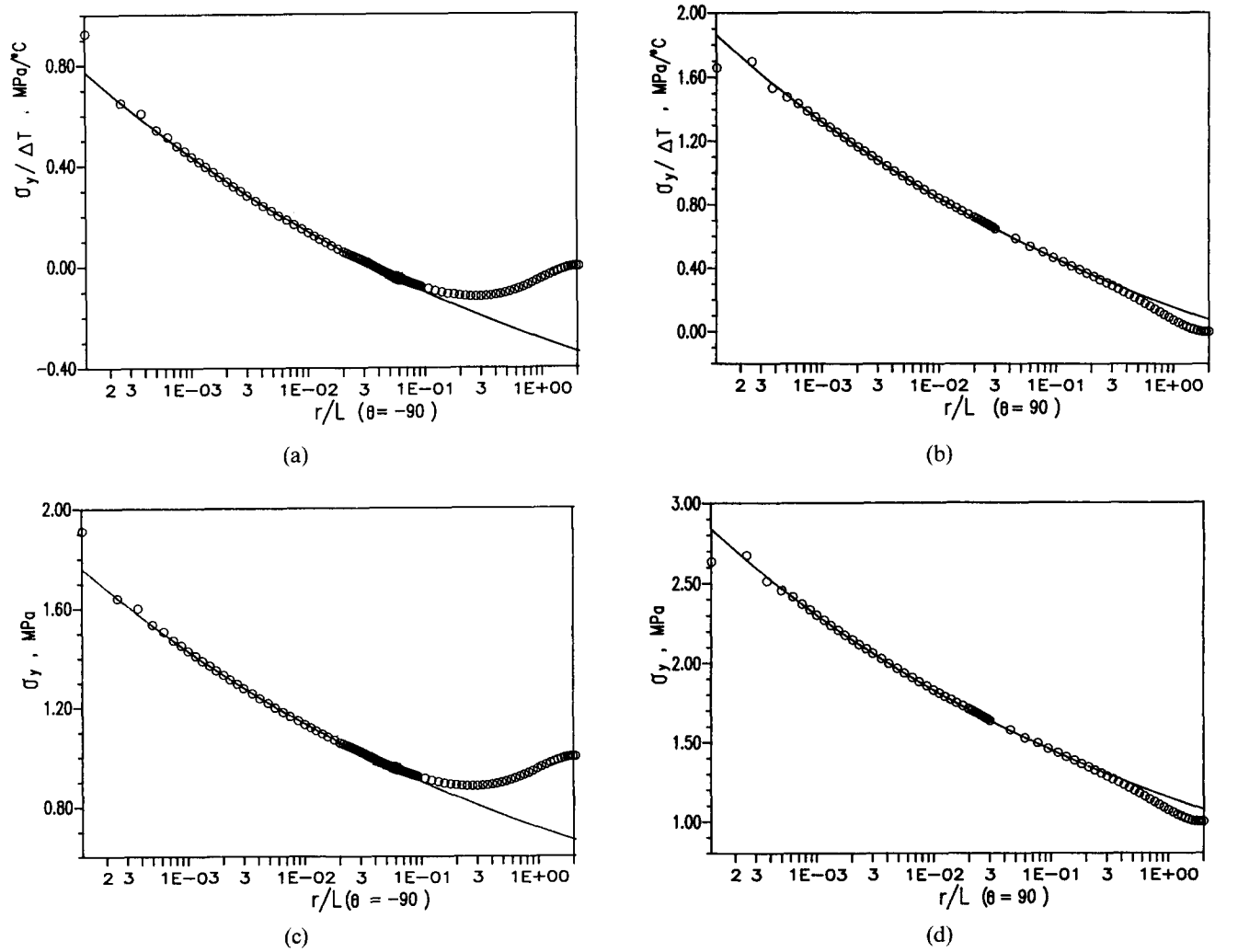

Fig. 6. Comparison of finite element results with analytical results (a), (b) under thermal loading; (c), (d) under mechanical loading (Al_2O_3/Ti–6Al–4V). Eqn (1); ○, FEM.

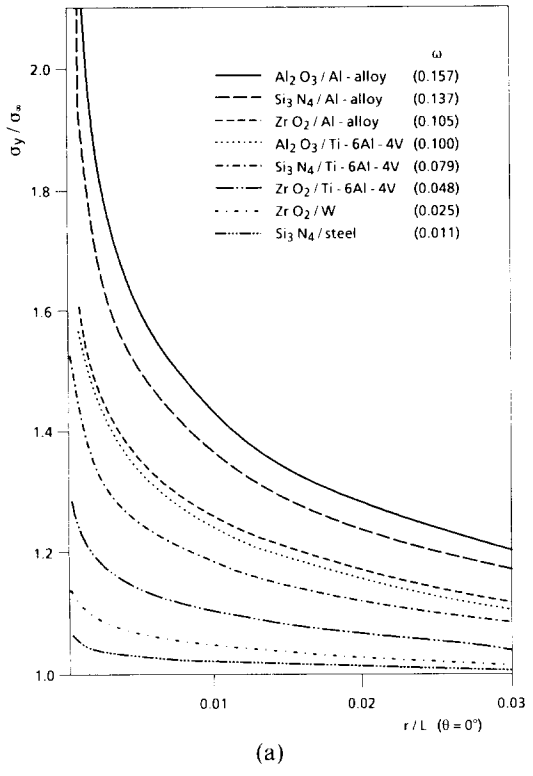

(a)

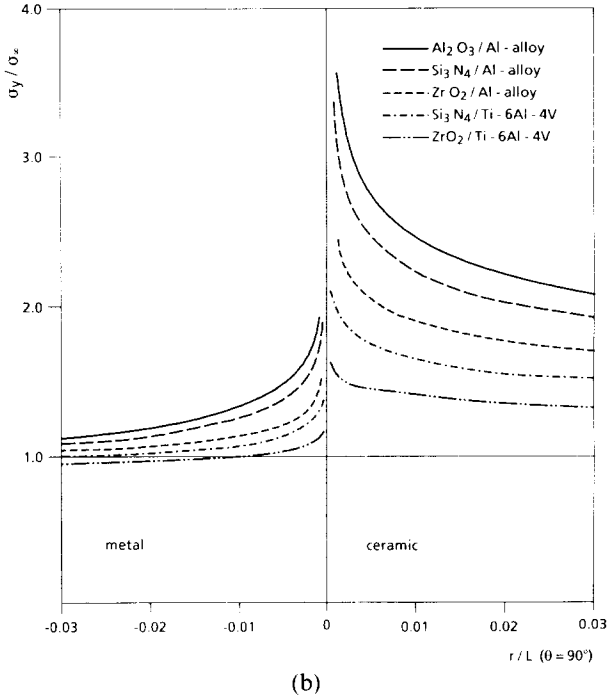

(b)

Fig. 7. Stresses along (a) the interface and (b) the free edge for different material combinations exposed to mechanical loading.

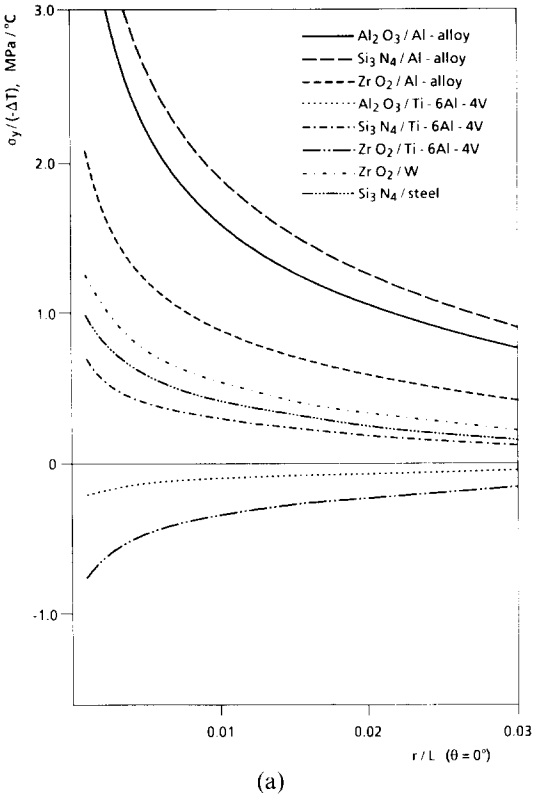

(a)

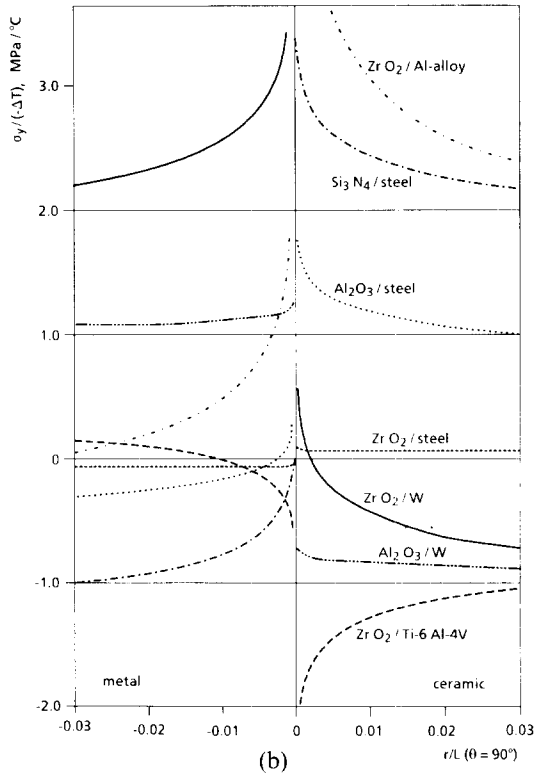

(b)

Fig. 8. Stresses along (a) the interface and (b) the free edge for different material combinations exposed to thermal loading.

zero. According to eqn (5) the ratio of the stress intensity factor to the applied stress decreases with increasing ω. This decrease, however, is overcome by the r^ω term. Also along the free edge the general trend is visible, that the stresses increase with increasing ω. In the ceramic this effect is even larger than that for the stresses acting along the interface, because the term f_r for $\theta = 90°$ also increases with ω. There is, however, no unique correlation with ω. The stresses are always larger in the material with the higher Young's modulus.

Results from eqns (1)–(5) are plotted in Fig. 8 for a change in temperature. To discuss these curves eqns (1), (4) and (5) are combined to read

$$\sigma_{ij} = -\Delta T \,.\, \Delta\alpha \,.\, \left[\frac{1}{E_1^*} - \frac{1}{E_2^*}\right]^{-1} \left[\frac{-K_L/\sigma_0}{(r/L)^\omega} f_{ij} - f_{ijo}\right] \quad (7)$$

It can be seen that the sign of the stresses depends mainly on the difference of the effective Young's

Table 2. Sign of stresses in material 1 (ceramic) after cooling from stress-free state

		Example
$\alpha_c^* > \alpha_M^*$ $E_c^* > E_M^*$	Compressive	Al_2O_3/Ti–6Al–4V Zr_2O_3/Ti–6Al–4V
$\alpha_c^* > \alpha_M^*$ $E_c^* < E_M^*$	Tensile (changes to compressive along free edge	Zr_2O_3/W Al_2O_3/W
$\alpha_c^* < \alpha_M^*$ $E_c^* > E_M^*$	Tensile	Al_2O_3/Cu Zr_2O_3/Cu Al_2O_3/steel Si_3N_4/steel
$\alpha_c^* < \alpha_M^*$ $E_c^* < E_M^*$	Compressive (Changes to tensile along free edge)	Si_3N_4/W

moduli and on the difference of the effective thermal expansion coefficients. For σ_y the last term in eqn (7) is always positive very close to the free edge of the interface. However, there might be a change in the sign of this term at some distance from the free edge of the interface. This change of the sign of the stress component σ_y occurs at very low values of r/L near the free edge in the material with the lower effective Young's modulus. The rules of the sign of the stresses in material 1 (ceramic) are given in Table 2 together with some examples.

4 Assessment of the stresses

The high stresses near the free edge of the interface may cause failure of the interface or of the ceramic. Very often, failure starts in the ceramic near the interface. No straightforward method exists for predicting the failure stress under mechanical loading or the critical change in the temperature in case of failure. One possibility of prediction consists in the application of the multiaxial Weibull theory as developed by Batdorf & Heinisch.[6] However, the high stress gradients give rise to some fundamental problems concerning the application of this theory. For assessment and comparison of different joints Kroupa *et al.*[7] proposed a value which is obtained by calculation of an average stress along a small distance from the free edge of the interface:

$$H_{ij} = \frac{1}{r^*/L} \int_0^{r^*/L} \sigma_{ij}(r)\Big|_{\theta = const.} \mathrm{d}(r/L)$$

$$= \frac{K_L f_{ij}}{(1-\omega)(r^*/L)^{\omega}} + \sigma_0 f_{ij0} \qquad (8)$$

In Table 3 these stresses are compiled for some joints. Thermal and mechanical averaged stresses

Table 3. Factor *Hy* for different material combinations (in MPa for mechanical loading and MPa/°C for thermal loading)

Materials	*Mechanical*		*Thermal*		ω	
	$\theta = 0°$	$\theta = 90°$	$\theta = 0°$	$\theta = 90°$		
Al_2O_3/Al alloy	2·44	4·20	5·35	11·9	0·157	$E_1^* > E_2^*$
Si_3N_4/Al alloy	2·17	3·55	6·10	13·4	0·137	$\alpha_1^* < \alpha_2^*$
ZrO_2/Al alloy	1·80	2·70	2·73	5·83	0·105	
Si_3N_4/Ti–6Al–4V	1·54	2·15	0·88	1·86	0·079	
Al_2O_3/steel	1·13	1·31	0·75	1·75	0·024	
Si_3N_4/steel	1·06	1·16	1·23	3·33	0·011	
ZrO_2/steel	1·00	1·005	0·004	0·06	0·000 26	
ZrO_2/W	1·139	1·045	1·58	0·52	0·025	$E_1^* < E_2^*$
Al_2O_3/W	1·004	0·99	0·20	0·72	0·000 36	$\alpha_1^* > \alpha_2^*$
Al_2O_3/Ti–6Al–4V	1·74	2·56	−0·75	−1·59	0·100	$E_1^* > E_2^*$
ZrO_2/Ti–6Al–4V	1·29	1·64	−0·95	−2·07	0·048	$\alpha_1^* > \alpha_2^*$
Si_3N_4/W	1·03	0·98	−0·25	0·147	0·005 6	$E_1^* < E_2^*$ $\alpha_1^* < \alpha_2^*$

along the interface and along the free edge are listed. The mechanical stresses are related to the applied stress σ_∞ and the thermal stresses are valid for cooling by one degree. The stresses have been averaged over a relative length of $r^*/L = 0{\cdot}001$.

5 Conclusions

The results for the stresses near the free edge in a bi-material joint with contact angle of 90° can be summarised as follows:

—The stresses can be described by eqn (1), with $\sigma_0 = 0$ for mechanical loading.

—The stress exponent ω and the angular functions f_{ij} are dependent on the two Dundurs parameters, which are functions of the Young's moduli and the Poisson's ratios of both materials.

—In the case of a change in temperature the stresses and thus the stress intensity factor K_L and the constant stress term σ_0 are proportional to the change in temperature ΔT, and proportional to the difference in the effective thermal expansion coefficients.

—The ratio between the stress intensity factor K_L and the applied stress σ_∞ for mechanical loading, and between K_L and the constant stress term σ_0 for a change in temperature is a unique function of the stress exponent ω.

—The stresses near the free edge of the interface after cooling from a stress free state are tensile for $E_1^* > E_2^*$ and $\alpha_1^* < \alpha_2^*$, or $E_1^* < E_2^*$ and $\alpha_1^* > \alpha_2^*$ and compressive for $E_1^* > E_2^*$ and $\alpha_1^* > \alpha_2^*$ or $E_1^* < E_2^*$ and $\alpha_1^* < \alpha_2^*$.

References

1. Bogy, D. B., Two edge-bonded elastic wedges of different materials and wedge angles under surface tractions. *J. Appl. Mech.*, **38** (1971) 377–89.
2. Williams, M. L., Stress singularities resulting from various boundary conditions in angular corners of plates in extension. *J. Appl. Mech.*, **19**, (1952) 526–8.
3. Suga, T., Mizuno, K. & Miyazawa, K., Thermal stresses in ceramic-to-metal joints. In *Proc. of the MRS Meeting on Advanced Materials*, Vol. 8. Materials Research Society, 1989, pp. 137–42.
4. Munz, D. & Yang, Y. Y., Stress singularities at the interface in bonded dissimilar materials under mechanical and thermal loading. *J. Appl. Mech.*, **59** (1992) 857–61.
5. Yang, Y. Y., Spannungssingularitäten in Zweistoffverbunden bei mechanischer und thermischer Belastung. Fortschritt-Bericht VDI, Reihe 18, No. 113, 1992.
6. Batdorf, S. B. & Heinisch, H. L., Weakest link theory reformulated for arbitrary fracture criterion. *J. Amer, Ceram. Soc.*, **61** (1978) 355–8.
7. Kroupa, F., Knesel, Z. & Zemankova, J., Criteria for crack propagation at ceramic interfaces. In *Proc. Int. Conf. Engineering Ceramics '92*, Smolnice Castle, ed. M. Haviar. 1992, pp. 102–9.

Appendix

(I) Determination of the stress exponent ω

$$(\omega-2)\left\{\beta^2\left[\cos^2\left(\frac{\pi}{2}\omega\right)-(\omega-1)^2\right]^2+\alpha^2\omega(\omega-1)^2(\omega-2)+2\alpha\beta(\omega-1)^2\left[\cos^2\left(\frac{\pi}{2}\omega\right)-(\omega-1)^2\right]+\cos^2\left(\frac{\pi}{2}\omega\right)\sin^2\left(\frac{\pi}{2}\omega\right)\right\}=0 \tag{A1}$$

where α, β are Dundurs parameters

$$\alpha=\frac{m_2-km_1}{m_2+km_1}$$

$$\beta=\frac{(m_2-2)-k(m_1-2)}{m_2+km_1}$$

with

$$k=\frac{G_2}{G_1}$$

$$m=\begin{cases}\dfrac{4}{(1+\upsilon)} & \text{for plane stress}\\[2ex] 4(1-\upsilon) & \text{for plane strain}\end{cases}$$

(II) Determination of the angular functions $f_{ij}(\theta)$

The angular functions are calculated by

$$\begin{aligned}f_{jr}(\theta)=\{&A_j(2+\omega)\sin(\omega\theta)\\&+B_j(2+\omega)\cos(\omega\theta)\\&-C_j(2-\omega)\sin[(2-\omega)\theta]\\&-D_j(2-\omega)\cos[(2-\omega)\theta]\}/\\&\{(2-\omega)(B_j+D_j)\}\end{aligned} \tag{A2}$$

$$\begin{aligned}f_{j\theta}(\theta)=\{&A_j\sin(\omega\theta)\\&+B_j\cos(\omega\theta)+C_j\sin[(2-\omega)\theta]\\&+D_j\cos[(2-\omega)\theta]\}/(B_j+D_j)\end{aligned} \tag{A3}$$

$$\begin{aligned}f_{jr\theta}(\theta)=-\{&A_j\omega\cos(\omega\theta)-B_j\omega\sin(\omega\theta)\\&+C_j(2-\omega)\cos[(2-\omega)\theta]\\&-D_j(2-\omega)\sin[(2-\omega)\theta]\}/\\&\{(2-\omega)(B_j+D_j)\ (j=1,2)\}\end{aligned} \tag{A4}$$

The coefficients are determined by

$$A_j=\frac{A_j^*}{X}\quad B_j=\frac{B_j^*}{X}\quad C_j=\frac{C_j^*}{X}\quad D_j=\frac{D_j^*}{X} \tag{A5}$$

with

$$X=\beta\left[\cos^2\left(\frac{\pi}{2}\omega\right)+(\omega-1)(\omega-3)\right]-\alpha(\omega-2)(\omega-1)-1+\cos^2\left(\frac{\pi}{2}\omega\right) \tag{A6a}$$

$$A_1^*=X \tag{A6b}$$

$$B_1^*=-\tan\left(\frac{\pi}{2}\omega\right)\left\{\beta\left[\cos^2\left(\frac{\pi}{2}\omega\right)+(\omega-1)^2\right]-\alpha(\omega-2)(\omega-1)+\cos^2\left(\frac{\pi}{2}\omega\right)\right\} \tag{A6c}$$

$$C_1^*=\beta\left[\frac{4-3\omega}{\omega-2}\sin^2\left(\frac{\pi}{2}\omega\right)-(\omega-2)\omega\right]+\alpha\omega(\omega-1)+\sin^2\left(\frac{\pi}{2}\omega\right) \tag{A6d}$$

$$D_1^*=\tan\left(\frac{\pi}{2}\omega\right)\left\{\frac{\beta}{\omega-2}\times\left[\cos^2\left(\frac{\pi}{2}\omega\right)(3\omega-4)-\omega(\omega-1)^2\right]+\alpha\omega(\omega-1)-\cos^2\left(\frac{\pi}{2}\omega\right)\right\} \tag{A6e}$$

$$\begin{aligned}A_2^*=-\frac{1}{1+\alpha}\Big\{&\alpha^2(\omega-2)(\omega-1)(2\omega-1)\\&+2\beta^2\left[(\omega-2)\sin^2\left(\frac{\pi}{2}\omega\right)+(\omega-2)^2\omega\right]\\&+\alpha\beta\left[\cos^2\left(\frac{\pi}{2}\omega\right)(2\omega-3)-4(\omega-2)^3\right.\\&\left.-9(\omega-2)^2-6(\omega-2)-1\right]\\&+\alpha\left[-\cos^2\left(\frac{\pi}{2}\omega\right)(2\omega-3)+(\omega-2)^2\right.\\&\left.+3(\omega-2)+1\right]\\&+\beta\left[-\sin^2\left(\frac{\pi}{2}\omega\right)(2\omega-3)+(\omega-2)^2\right]\\&+\sin^2\left(\frac{\pi}{2}\omega\right)\Big\}\end{aligned} \tag{A6f}$$

$$B_2^* = -\frac{\tan\left(\frac{\pi}{2}\omega\right)}{1+\alpha}\Big\{\alpha^2(\omega-2)(\omega-1)(2\omega-1)$$
$$+2\beta^2\Big[-(\omega-1)\cos^2\left(\frac{\pi}{2}\omega\right)+(\omega-2)^3$$
$$+3(\omega-2)^2+3(\omega-2)+1\Big]$$
$$+\alpha\beta\Big[\cos^2\left(\frac{\pi}{2}\omega\right)(2\omega-3)-4(\omega-2)^3$$
$$-11(\omega-2)^2-10(\omega-2)-3\Big]$$
$$+\alpha\Big[-\cos^2\left(\frac{\pi}{2}\omega\right)(2\omega-3)-(\omega-2)^2-(\omega-2)\Big]$$
$$+\beta\Big[\cos^2\left(\frac{\pi}{2}\omega\right)(2\omega-3)+(\omega-2)^2+(2\omega-3)\Big]$$
$$+\cos^2\left(\frac{\pi}{2}\omega\right)\Big\} \tag{A6g}$$

$$C_2^* = -\frac{1}{1+\alpha}\Big\{\alpha^2\omega\Big[2(\omega-2)^2+3(\omega-2)+1\Big]$$
$$+2\beta^2\omega\Big[-\cos^2\left(\frac{\pi}{2}\omega\right)+(\omega-2)^2+2(\omega-2)+1\Big]$$
$$+\frac{\alpha\beta}{\omega-2}\Big[\cos^2\left(\frac{\pi}{2}\omega\right)(2\omega^2-5\omega+4)$$
$$-4\omega^4+17\omega^3-26\omega^2+17\omega-4\Big]$$
$$+\alpha\Big[\cos^2\left(\frac{\pi}{2}\omega\right)(1-2\omega)-(\omega-2)^2-(\omega-2)+1\Big]$$
$$+\frac{\beta}{\omega-2}\Big[\cos^2\left(\frac{\pi}{2}\omega\right)(2\omega^2-5\omega+4)$$
$$+\omega^3-6\omega^2+9\omega-4\Big]-\sin^2\left(\frac{\pi}{2}\omega\right)\Big\} \tag{A6h}$$

$$D_2^* = \frac{\tan\left(\frac{\pi}{2}\omega\right)}{1+\alpha}\Big\{\alpha^2\omega\Big[2(\omega-2)^2+3(\omega-2)+1\Big]$$
$$+2\beta^2\Big[-(\omega-1)\cos^2\left(\frac{\pi}{2}\omega\right)+(\omega-2)^3$$
$$+3(\omega-2)^2+3(\omega-2)+1\Big]$$
$$+\frac{\alpha\beta}{\omega-2}\Big[\cos^2\left(\frac{\pi}{2}\omega\right)(2\omega^2-5\omega+4)-4\omega^4$$
$$+19\omega^3-34\omega^2+27\omega-8\Big]$$
$$+\alpha\Big[\cos^2\left(\frac{\pi}{2}\omega\right)(1-2\omega)+\omega(\omega-1)\Big]$$
$$+\frac{\beta}{\omega-2}\Big[\cos^2\left(\frac{\pi}{2}\omega\right)(2\omega^2-5\omega+4)$$
$$-\omega(\omega-1)^2\Big]-\cos^2\left(\frac{\pi}{2}\omega\right)\Big\} \tag{A6i}$$

$$f_{r0} = \sin^2(\theta) \tag{A7a}$$

$$f_{\theta 0} = \cos^2(\theta) \tag{A7b}$$

$$f_{r\theta 0} = \cos(\theta)\sin(\theta) \tag{A7c}$$